High Power Laser Science and Engineering, (2023), Vol. 11, e65, 4 pages.
doi:10.1017/hpl.2023.60

RESEARCH ARTICLE

Kilowatt-class high-energy frequency conversion to 95 J at 10 Hz at 515 nm

Martin Divoky[1], Jonathan Phillips[2], Jan Pilar[1], Martin Hanus[1], Petr Navratil[1], Ondrej Denk[1], Tomas Paliesek[1], Patricie Severova[1], Danielle Clarke[2], Martin Smrz[1], Thomas Butcher[2], Chris Edwards[2], John Collier[2], and Tomas Mocek[1]

[1] *HiLASE Centre, Institute of Physics of the Czech Academy of Sciences, Dolni Brezany, Czech Republic*

[2] *Central Laser Facility, STFC Rutherford Appleton Laboratory, Didcot, UK*

(Received 24 March 2023; revised 19 May 2023; accepted 13 July 2023)

Abstract

We report on frequency doubling of high-energy, high repetition rate ns pulses from a cryogenically gas cooled multi-slab ytterbium-doped yttrium aluminum garnet laser system, Bivoj/DiPOLE, using a type-I phase matched lithium triborate crystal. We achieved conversion to 515 nm with energy of 95 J at repetition rate of 10 Hz and conversion efficiency of 79%. High conversion efficiency was achieved due to successful depolarization compensation of the fundamental input beam.

Keywords: diode pumped solid state laser; frequency conversion; high energy; high average power

1. Introduction

Frequency conversion of high-energy, high average power (HE-HAP) diode pumped laser systems opens up new applications from underwater laser shock peening of complex samples[1] and laser induced damage testing at broader wavelength ranges to pumping of Ti:sapphire and optical parametric chirped pulse amplification (OPCPA) systems[2–4]. Recently, the HE-HAP frequency conversion has gained even more importance due to the success of inertial confinement fusion experiments[5].

Currently, many laser systems with second harmonic conversion operate at, or above, kilowatt average power, but only with low pulse energy of a few mJ[6] or J[7]. The highest energy achieved around wavelength of 500 nm on a high average power system before this work was 60 J[8].

In this paper we report second harmonic generation (SHG) of 95 J at a repetition rate of 10 Hz from the laser system Bivoj/DiPOLE[9,10], which corresponds to 950 W of average power. It is, to the best of our knowledge, the highest average power in a high-energy system with energy of more than 1 J with a wavelength around 500 nm and corresponds to 58% increase in the state-of-the-art. Conversion efficiency of 79% was achieved by using flat top beam and pulse profiles and by successful optimization of depolarization by the polarimetric method[11].

2. Experiment

The output from a high average power ytterbium-doped yttrium aluminum garnet (Yb:YAG) laser system, Bivoj/DiPOLE, at 1030 nm was frequency converted to 515 nm using type-I phase matching in a lithium triborate (LBO) crystal. The LBO crystal (Coherent, Inc.) was optimized for SHG from 1030 nm laser radiation. The crystal had an aperture of 60 mm × 60 mm, thickness of 13 mm and cut angle theta of 90° and phi of 13.6°. Dual band anti-reflection (AR) coatings of 1030 and 515 nm were used on both faces to minimize total transmission losses to 0.25% and 0.75%, respectively. The crystal was placed into a windowless oven (IB Photonics) for temperature stabilization. The temperature was set to 30°C. Higher temperatures provided better conversion stability, as the oven uses ambient air to cool down the crystal, but with a lower conversion efficiency, because the large difference between the ambient temperature and the oven temperature

Correspondence to: Martin Divoky, HiLASE Centre, Institute of Physics of the Czech Academy of Sciences, Za Radnici 828, 25241 Dolni Brezany, Czech Republic. Email: divoky@fzu.cz

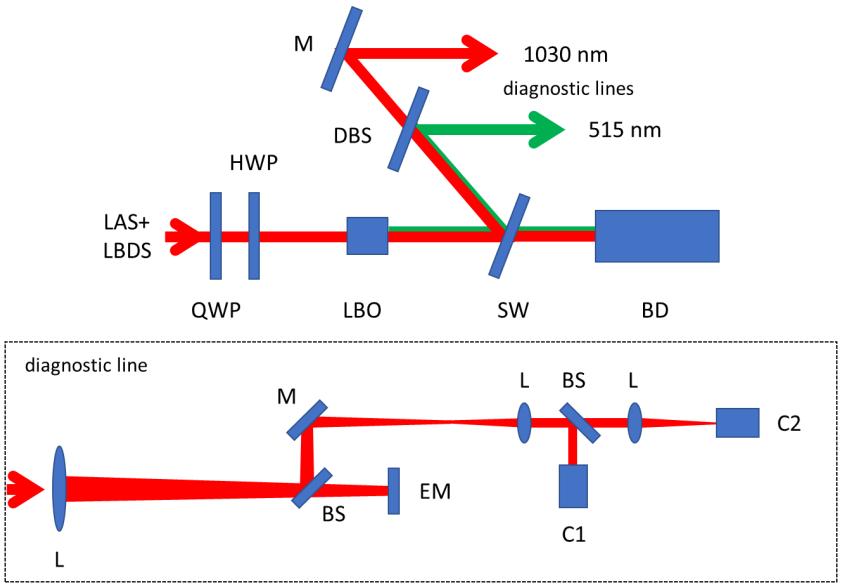

Figure 1. Schematic layout of the conversion experiment. It consists of a laser system and laser beam distribution system (LAS+LBDS), quarter waveplate (QWP), half waveplate (HWP), conversion crystal (LBO), partially reflecting sampling wedge (SW) and beam dump (BD). The diagnostics consist of a dichroic beamsplitter (DBS), mirrors (M), lenses (L), beamsplitters (BS), an energy meter (EM), a near-field camera (C1) and a far field camera (C2). The layout of diagnostic lines is the same for both wavelengths and is shown only once.

creates higher temperature gradients in the crystal. A laser beam from the laser system is propagated to the harmonic conversion setup through a series of telescopes. They demagnify the laser beam 1.56 times from 77 mm × 77 mm to 49 mm× 49 mm to increase the energy fluence on the crystal. The layout of the harmonic conversion setup can be seen in Figure 1. A pair of zero-order waveplates (λ/2, λ/4) was used to adjust the polarization at the input of the crystal to improve the conversion efficiency by maximizing the energy in the polarization parallel with the principal plane of the crystal. After passing through the crystal, the high-power beam containing unconverted fundamental and converted second harmonic beams was terminated in a water-cooled absorption beam dump. The 1030 nm light was absorbed in water and the 515 nm light was absorbed in colored glass filters suspended in a water tank. Glass plates with different absorption bands were used to distribute the energy absorption equally among them. In front of the beam dump, a sampling wedge (dielectrically coated $R \sim 1\%$ at 1030 and 515 nm) was placed so that a low-power reflection could be acquired and used for diagnostics. The diagnostic beam was divided according to wavelength by a dichroic mirror. Each diagnostic line contained an energy meter (Gentec-EO QE25LP) and diagnostic cameras (AVT Manta 145B) to monitor the image-relayed beam profiles.

The laser was operated with output energy of 130 J at a repetition rate of 10 Hz. The pulse duration of the flat top pulses was 10 ns with a rise/fall time of 0.75 ns. The spectrum was centered at 1029.8 nm and the bandwidth was around 1 pm. The polarization homogeneity was not uniform across the beam. The main reason for this is the heat dissipated in the amplifier head that generates stresses in the Yb:YAG gain media that create birefringence and change the polarization state of the beam with spatial variability over the beam cross-section. This polarization change is sometimes referred to as depolarization, although this term should be reserved for cases where polarized light is changed into non-polarized light. When this beam propagates through a linear polarizer, a portion of its energy is inevitably rejected, and this contributes to energy losses. In the main power amplifier of Bivoj, these losses can be as high as 50% (Figures 2(a) and 2(b)) if linear polarization is used at the amplifier input and without waveplates at the output. We placed a pair of zero-order waveplates (λ/2, λ/4) after the Faraday isolator after the main cryogenic pre-amplifier (10 J) of the Bivoj/DiPOLE system to change the input linear polarization into the main cryogenic power amplifier (100 J); the output polarization was adjusted by a similar pair in the harmonic conversion setup. By tweaking the input polarization only, the energy losses are decreased to 35% (Figures 2(c) and 2(d)). If only the output polarization is optimized, the energy losses decrease further to 32% (Figures 2(e) and 2(f)). By using a custom polarimetric technique to evaluate the Mueller matrix of the Bivoj system[11], we were able to estimate numerically the optimal input polarization to further decrease the energy losses to around 3% (Figures 2(g) and 2(h)). These results were obtained for output energy of 90 J, helium flow rate of 150 gps (gallons per second) and temperature of 120 K. We optimized the polarization homogeneity at lower energy output to avoid changes to the beam, as the maximum output energy is close to laser induced damage threshold of the

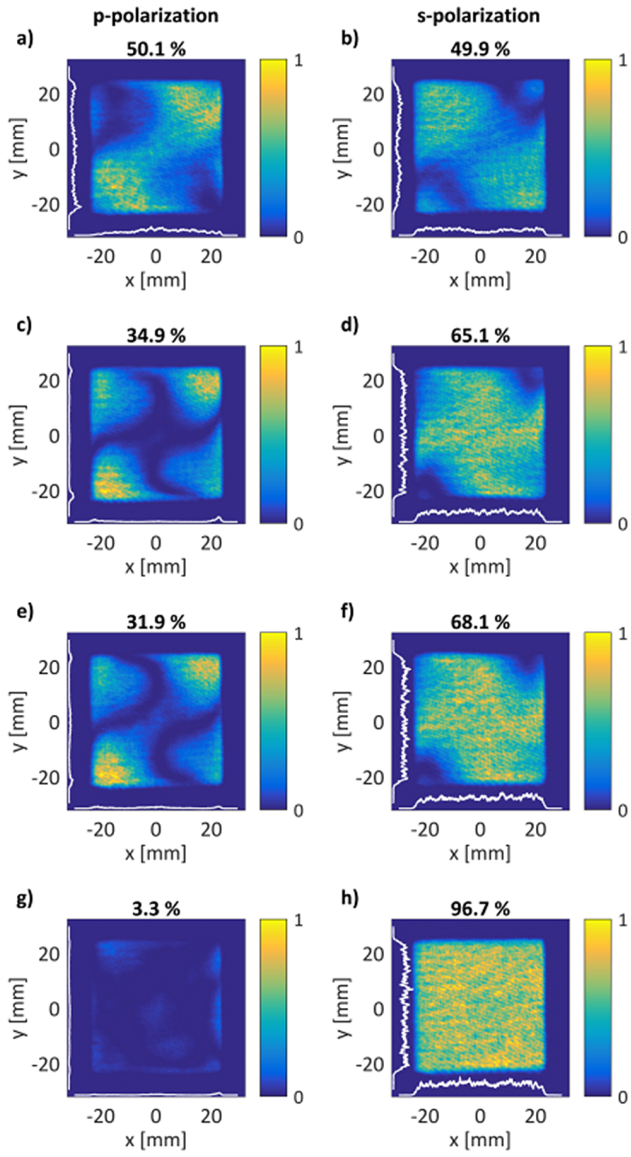

Figure 2. Beam profiles after correction waveplates after polarizer transmitting vertical polarization (a), (c), (e), (g) or horizonal polarization (b), (d), (f), (h). (a), (b) Linear polarization entering the power amplifier with no optimization at the output. (c), (d) Optimized polarization at the input. (e), (f) Linear polarization at the input and optimized polarization at the output. (g), (h) Optimized polarization at the input and output. Beam profiles at complementary polarizations were taken under the same conditions and were normalized to the sum of both intensities. The white lines in the pictures correspond to cross-lines through the center of the beam.

optical components. The pump energy was adjusted to operate at the maximum energy extraction from the amplifier. At the maximum output energy of 130 J, we used more intense pumping and increased the flow rate to 180 gps. We adjusted the polarization homogeneity by slightly tweaking all waveplates and the energy losses dropped from around 5% to around 3% with similar profiles as in Figures 2(g) and 2(h). Once the polarization homogeneity was optimized, it did not require any adjustments at the given energy output. Note that vertical polarization is used for SHG.

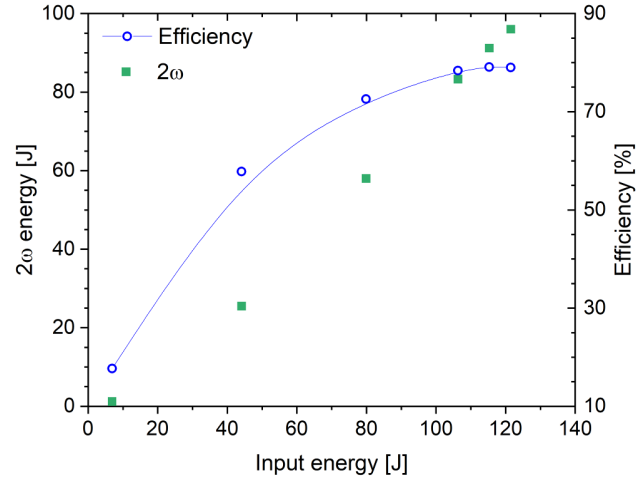

Figure 3. Dependence of the second harmonic frequency output energy and conversion efficiency on the input energy during the energy ramp in the beginning of the experiment.

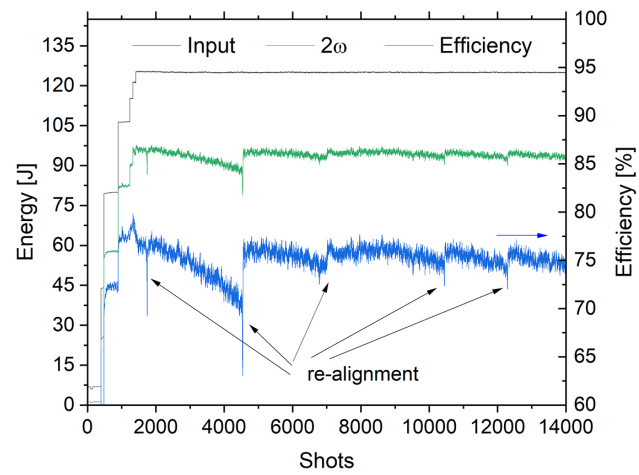

Figure 4. Temporal evolution of the energy of the second harmonic frequency and conversion efficiency. Points where the crystal phase matching angle was optimized are marked with arrows.

After the optimization of polarization homogeneity, the LBO crystal was inserted into the position and aligned using a low-energy beam. Then the energy was gradually increased up to 130 J at the output of the laser (121 J on the crystal; the transmission of the optics from the output of the laser to the LBO crystal was 93.4%) and the phase matching angles were optimized. Energy conversion and conversion efficiency dependence are shown in Figure 3 and the temporal development is shown in Figure 4. The energy of SHG at 515 nm reached the value of 96 J and the conversion efficiency of 79% $\pm$ 0.6%. If we would count only the input energy on the polarization that is converted to the second harmonic (i.e., neglect the depolarization losses), the conversion efficiency would reach 81.5% $\pm$ 0.6%. Since the oven controls the temperature of the crystal holder, after the beam is propagated through the crystal, the absorption causes the average temperature of the crystal to rise above

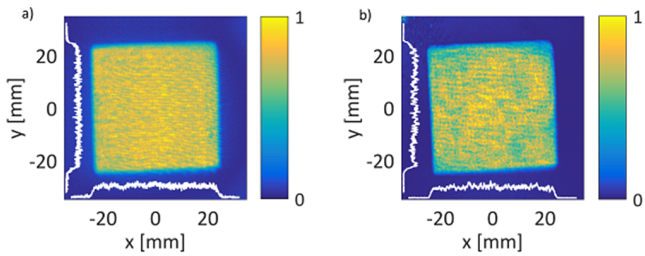

Figure 5. Near-field beam profiles of the input beam at 1030 nm with energy of 121 J and the converted second harmonic frequency (515 nm) beam with energy of 95 J at the repetition rate of 10 Hz.

the set temperature. During this thermalization of the crystal, the converted energy and efficiency dropped, so we re-aligned the phase matching angles several times. While we could compensate for the overall temperature increase in the crystal by adjusting the phase matching angle, the induced temperature gradients could not be compensated for in such a way. Therefore, the output energy dropped to 94–95 J with conversion efficiency of 76% ± 0.6%, because of the temperature gradients. Converted energy steadily decreased over time because of the overall temperature increase, on the order of minutes, but it could be recovered by consecutive phase matching angle optimization. Energy stability of the input beam at fundamental frequency was 0.1% RMS (root mean square) and 0.6% P-t-P (peak-to-peak). The energy stability of the second harmonic beam at the beginning of the experiment was 1.5% RMS and 8% P-t-P (shots 1900–4100) and was caused by rapid heating of the crystal. After thermalization of the crystal and re-optimization of the phase matching, the energy stability improved to 0.8% RMS and 6% P-t-P (shots 7500–10,000). A further increase in energy stability could be achieved by improving the temperature control of the crystal or automatic phase matching angle optimization, which will be studied in detail in future work. The near-field beam profile of the input beam on the fundamental frequency and the corresponding converted beam at the energy of 95 J is shown in Figures 5(a) and 5(b).

3. Conclusion

The output of SHG of 95 J at 10 Hz at 515 nm was achieved for the first time and represents a 58% increase to the state-of-the-art. The SHG process was achieved using an LBO crystal placed in a temperature-controlled holder. The good uniformity of the near-field profile of the converted beam and high conversion efficiency has been achieved mainly by addressing the problem of stress induced non-uniform polarization changes originating from within the amplifier chain and their successful mitigation. The reported energy stability of SHG output is of the order of 0.8% RMS, which is below the laser performance capability and is caused mainly by the unstable temperature within the LBO crystal due to the high average power nature of the working beam. The instability of the crystal temperature will be addressed in the future by optimized design of the temperature stabilization controller.

Acknowledgements

This work was supported by the European Regional Development Fund and the state budget of the Czech Republic project HiLASE CoE (CZ.02.1.01/0.0/0.0/15_006/0000674) and the Horizon 2020 Framework Programme (H2020) (739573).

References

1. Y. Sano, N. Mukai, M. Yoda, T. Uehara, I. Chida, and M. Obata, Proc. SPIE **6343**, 634324 (2006).
2. C. L. Haefner, A. Bayramian, S. Betts, R. Bopp, S. Buck, J. Cupal, M. Drouin, A. Erlandson, J. Horacek, J. Horner, J. Jarboe, K. Kasl, D. Kim, E. Koh, L. Koubikova, W. Maranville, C. Marshall, D. Mason, J. Menapace, P. Miller, P. Mazurek, A. Naylon, J. Novak, D. Peceli, P. Rosso, K. Schaffers, E. Sistrunk, D. Smith, T. Spinka, J. Stanley, R. Steele, C. Stolz, T. Suratwala, S. Telford, J. Thoma, D. VanBlarcom, J. Weiss, and P. Wegner, Proc. SPIE **10241**, 1024102 (2017).
3. https://www.clf.stfc.ac.uk/Pages/EPAC-introduction-page.aspx.
4. G. Archipovaite, M. Galletti, P. Oliveira, M. Ahmad, R. Clarke, D. Neely, N. Booth, R. Heathcote, M. Galimberti, I. Musgrave, and C. Hernandez-Gomez, in 2019 *Conference on Lasers and Electro-Optics Europe and European Quantum Electronics Conference* (Optica Publishing Group, 2019), paper ca_2_2.
5. https://www.llnl.gov/news/national-ignition-facility-achieves-fusion-ignition.
6. C. Röcker, A. Loescher, F. Bienert, P. Villeval, D. Lupinski, D. Bauer, A. Killi, T. Graf, and M. A. Ahmed, Opt. Lett. **45**, 5522 (2020).
7. H. Chi, Y. Wang, A. Davenport, C. S. Menoni, and J. J. Rocca, Opt. Lett. **45**, 6803 (2020).
8. J. P. Phillips, S. Banerjee, P. Mason, J. Smith, J. Spear, M. De Vido, K. Ertel, T. Butcher, G. Quinn, D. Clarke, C. Edwards, C. Hernandez-Gomez, and J. Collier, Opt. Lett. **46**, 1808 (2021).
9. P. Mason, M. Divoký, K. Ertel, J. Pilař, T. Butcher, M. Hanuš, S. Banerjee, J. Phillips, J. Smith, M. De Vido, A. Lucianetti, C. Hernandez-Gomez, C. Edwards, T. Mocek, and J. Collier, Optica **4**, 438 (2017).
10. M. Divoký, J. Pilař, M. Hanuš, P. Navrátil, O. Denk, P. Severová, P. Mason, T. Butcher, S. Banerjee, M. De Vido, C. Edwards, J. Collier, M. Smrž, and T. Mocek, Opt. Lett. **46**, 5771 (2021).
11. O. Slezák, M. Sawicka-Chyla, M. Divoký, J. Pilař, M. Smrž, and T. Mocek, Sci. Rep. **12**, 18334 (2022).